Weierstraß-Institut
für Angewandte Analysis und Stochastik

im Forschungsverbund Berlin e.V.

Preprint ISSN 0946 – 8633

Electronic States in Semiconductor Nanostructures and Upscaling to Semi-Classical Models.

Thomas Koprucki, Hans-Christoph Kaiser, Jürgen Fuhrmann

Weierstrass Institute for Applied Analysis and Stochastics

koprucki@wias-berlin.de, kaiser@wias-berlin.de,fuhrmann@wias-berlin.de

submitted: May 12, 2006

No. 1133

Berlin 2006

2000 *Mathematics Subject Classification.* 82D37, 34L40.

Key words and phrases. Semiconductor Nanostructures, k·p Method, Electronic States, Band Structure, Semiclassical Models, Upscaling, Quantum Wells, Semiconductor Lasers.

Edited by
Weierstraß-Institut für Angewandte Analysis und Stochastik (WIAS)
Mohrenstraße 39
10117 Berlin
Germany

Fax: + 49 30 2044975
E-Mail: preprint@wias-berlin.de
World Wide Web: http://www.wias-berlin.de/

Electronic states in semiconductor nanostructures and upscaling to semi-classical models.

Thomas Koprucki, Hans-Christoph Kaiser, and Jürgen Fuhrmann

Weierstrass Institute for Applied Analysis and Stochastics,
Mohrenstraße 39, 10117 Berlin

koprucki@wias-berlin.de, kaiser@wias-berlin.de, fuhrmann@wias-berlin.de

1 Introduction

Nanostructures are one of the basic features of quantum electronic semiconductor devices. In order to cover quantum effects in semiconductor device simulation, one has to compute the states of the acting electrons and one has to incorporate adequate information about these electronic states into the device simulation tools, which usually operate on a semi-classical level.

In semiconductor devices one basically distinguishes three spatial scales: the atomistic scale of the bulk semiconductor materials (sub-Å), the scale of the interaction zone at the interface between two semiconductor materials together with the scale of the resulting size quantization (nanometer) and the scale of the device itself (micrometer).

At the ab-initio level, the many-body Schrödinger equation for the electrons in the potential of the nuclei gives a complete description of the electronic structure for a semiconductor bulk material. The electrons present in semiconductor materials can be subdivided into two classes: the core electrons and the valence electrons. On the energy scale, the core electrons have much lower levels than the valence electrons. This allows to decouple them from the valence electrons. Together with the nuclei, they form the ionic cores. The valence electrons are responsible for the chemical bonds and for many electronical and optical properties. The electronic states of the valence electrons can be described with high accuracy in the framework of density functional theory. This approach results in a one-particle Schrödinger equation on the *atomistic scale* with a potential given by the ionic cores and the mean field contribution of the interaction between the valence electrons.

The prototype semiconductor nanostructure is a quantum well structure which consists of a stack of different semiconductor materials grown on a substrate, see Fig. 2. The thickness of these layers usually ranges from 2

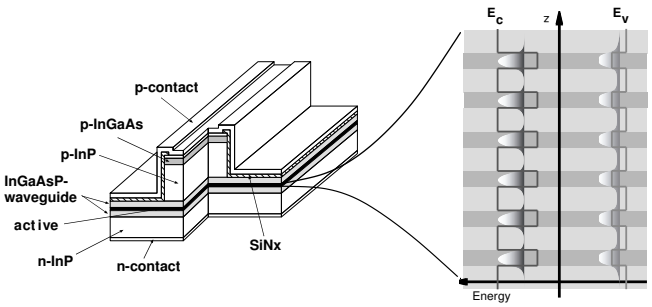

Fig. 1. Schema of a SMQW laser diode by HHI, Berlin. Holes injected from the p-contact and electrons injected from the n-contact recombine in the optical active region. The optical active region consisting of six quantum wells is enlarged on the right. E_c and E_v are the band edge profiles for the electrons and holes. The quantum confinement of the electrons and holes within the wells is indicated.

to 20 nm, defining the *nanoscale*. The characteristic feature of the material interface between two layers is the abrupt change of the parameters of the crystal (chemical composition, band structure) on a distance of the same order of magnitude as the lattice constant. Basically, this leads to a coupling of the electronic states of the different materials meeting at the interface. The variation of material properties across nanoscale heterostructures induces size-quantization.

The nanostructure is in the focus of the envelope function approximation, which can be understood as a homogenization method with Bloch waves. It leads to $k{\cdot}p$ multi-band Schrödinger-type equations with position-dependent effective mass tensor and band-edge profile, which are state of the art for the description of electronic states in semiconductor nanostructures.

Figure 1 shows the essential components of an edge-emitting strained multiple quantum well (SMQW) semiconductor laser diode, the optical active zone of which is a stack of quantum wells separated by barriers from a different material. The transversal simulation of such a laser deals with a cross section measuring up to several microns in diameter. Semi-classical models working on the *device scale* such as drift-diffusion equations are state of the art for the simulation of the electronic behavior of many microelectronic devices. For opto-electronic devices based on nanostructures they can be applied successfully, supposed the constitutive laws in these semi-classical models take into account quantum effects from smaller scale models for the embedded nanostructure [BGK00, BHK03, BKKR03, BGH05].

The present paper focuses on the two scale transitions inherent in the hierarchy of scales in the device. In section 2, we start with the description of the band structure of the bulk material by $k{\cdot}p$ Hamiltonians on the atomistic scale. Section 3 describes how the envelope function approximation allows

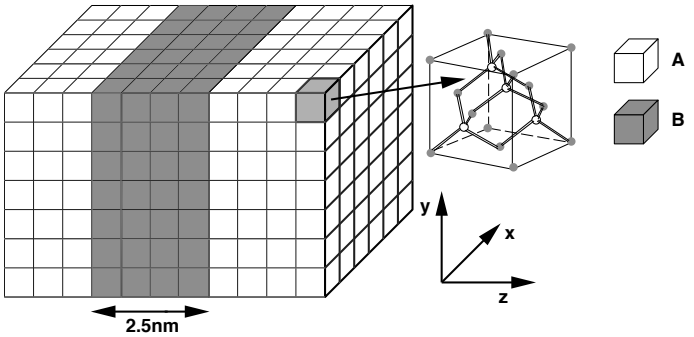

Fig. 2. Quantum well: one-dimensional semiconductor nanostructure consisting of two semiconductor materials A and B and two planar material interfaces. The unit cell for a binary semiconductor with zinc-blende crystallographic structure like gallium arsenide is displayed.

to construct kp Schrödinger operators describing the electronic states at the nanoscale which are closely related to the $k{\cdot}p$ Hamiltonians from section 2. Special emphasis is placed on the possible existence of spurious modes in the $k{\cdot}p$ Schrödinger model on the nanoscale which are inherited from anomalous band bending on the atomistic scale. Section 4 is devoted to the mathematical analysis of these multi-band $k{\cdot}p$ Schrödinger operators. Besides of the confirmation of the main facts about the band structure usually taken for granted, key results are conditions on the coefficients of the $k{\cdot}p$ Schrödinger operator for the nanostructure, which exclude spurious modes and an estimate of the size of the band gap. Section 5 gives an overview of properties of the electronic band structure of strained quantum wells. Further, the assumption of flat-band conditions across the nanostructure allows for upscaling of quantum calculations to state equations for semi-classical models. In section 6 we demonstrate this approach for parameters such as the quantum corrected band-edges, the effective density of states, the optical response, and the optical peak gain. Section 7 is devoted to the application of the $k{\cdot}p$ Schrödinger theory to low gap quantum wells, a case where a proper rescaling of the optical matrix element is necessary to avoid spurious modes. In Section 8 we discuss the application of the $k{\cdot}p$ Schrödinger models to biased quantum wells, the operation mode of electro-optic modulators.

2 Near-band-edge states in semiconductor bulk crystals

The key property of bulk semiconductor materials is, that the atoms form a periodic Bravis lattice defined by its crystallographic unit cell, see Fig. 2 and [Car96]. The electronic states of the valence electrons in a semiconductor are essentially given by the solution of the eigenvalue problem for a Schrödinger

operator

$$H = -\frac{\hbar^2}{2m_0}\Delta + V_{eff}(r). \tag{1}$$

m_0 is the electron rest mass and V_{eff} is the effective potential, consisting of the potential of ionic cores (nuclei and core electrons) and the mean field interaction between the valence electrons. This potential can be given by empirical pseudopotential method (EPM) [CB66, CC76, Car96]. Alternatively, density functional theory allows to obtain the electronic states by solving an effective one-particle Schrödinger equation with a periodic potential.

Due to the translation invariance of the lattice periodic potential, the eigenfunctions of the Schrödinger operator are Bloch waves

$$\Psi(r;k) = e^{\mathrm{i}kr}u(r;k), \tag{2}$$

defined by a lattice periodic Bloch function $u(r;k)$ depending on the real space vector $r = (x, y, z)$ and parametrically on the wave vector $k = (k_x, k_y, k_z)$, Bloch theorem see [Blo32, Car96]. The Bloch waves as well as the corresponding eigenvalue curves $E(k)$ are periodic in the wave vector k. Thus, it is sufficient (reduced zone scheme) to restrict the considerations to the first *Brillouin zone*, the unit cell of the periodic lattice in the k space, see [Car96].

2.1 $k{\cdot}p$ equation for Bloch waves

The Bloch wave ansatz (2) leads to an eigenvalue problem for the Bloch function $u(r;k)$ [Kan66, Kan82]. Including the spin degree of freedom by using a two-component Bloch function one arrives at the at the $k{\cdot}p$ equation. Using the notation of [Bah90] it reads as:

$$Hu_n(r;k) = E_n(k)u_n(r;k) \tag{3}$$

with

$$H = H_0 + H_{k\cdot p} + H_k + H_{so} + H_{kso}$$

$$H_0 = -\frac{\hbar^2}{2m_0}\Delta + V_{eff}(x), \quad H_{k\cdot p} = \frac{\hbar}{m_0}k\cdot p, \quad H_k = \frac{\hbar^2k^2}{2m_0},$$
$$H_{so} = \frac{\hbar}{4m_0^2c^2}\big((\nabla V_{eff})\times p\big)\cdot\sigma, \quad H_{kso} = \frac{\hbar^2}{4m_0^2c^2}\big((\nabla V_{eff})\times k\big)\cdot\sigma.$$

p denotes the quantum mechanical momentum operator defined by $p = -\mathrm{i}\hbar\nabla$. $\sigma = (\sigma_x, \sigma_y, \sigma_z)$ is the vector of the Pauli spin matrices

$$\sigma_x = \begin{pmatrix} 0 & 1 \\ 1 & 0 \end{pmatrix}, \quad \sigma_y = \begin{pmatrix} 0 & -\mathrm{i} \\ \mathrm{i} & 0 \end{pmatrix}, \quad \sigma_z = \begin{pmatrix} 1 & 0 \\ 0 & -1 \end{pmatrix}.$$

H_{so} and H_{kso} describe the spin-orbit interaction.

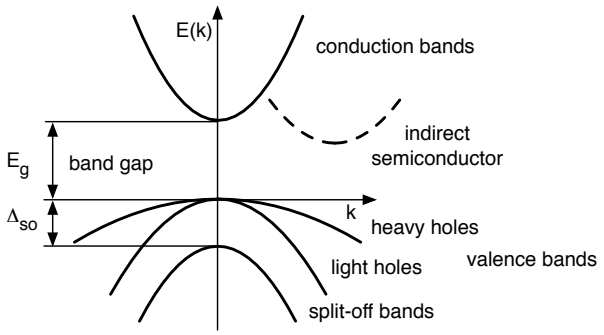

Fig. 3. Schematic of the band structure in a direct semiconductor material (the lowest conduction band and the three topmost valence bands). Due to the Kramers degeneracy (spin degeneracy) each state is doubly degenerate. For indirect semiconductor materials the conduction band minimum is located outside the zone-center $k = 0$ as indicated by the dashed line. Due to crystal symmetry there may exist multiple equivalent band minima in this case, for instance, six in silicon.

The eigenvalue curves $E_n(k)$ are the energy bands of the valence electrons in a semiconductor material. Together they form the electronic band structure. The essential property of the band structure in a semiconductor is the existence of a fundamental spectral gap. Energy bands below and above this gap are valence bands and conduction bands, respectively. For the cases of interest, the maximum E_v of the valence band is located at the Γ point, center $k = 0$ of the Brillouin zone. In direct semiconductor materials such as gallium arsenide, the minimum E_c of the conduction bands is also located at the Γ point, whereas for indirect semiconductors such as silicon, it is located outside the zone-center. The band-edges E_c and E_v define the band gap $E_g = E_c - E_v$. Fig. 3 shows a schematic band diagram. In thermodynamic equilibrium, the carriers occupy the states near the band extrema. In particular, the conduction band states are occupied by the free roaming electrons and the valence band states are occupied by the positively charged holes. Therefore, for many applications it is sufficient to confine the description of band structure to the near-band-edge states.

2.2 Eight-band $k{\cdot}p$ Hamiltonian for near band-edge states

Basically, any Bloch function $u(r, k)$ can be represented in terms of the zone-center solutions $u_n^\Gamma(r) = u_n(r, k = 0)$:

$$u_n(r, k) = \sum_{n'} C_{n'}(k) u_{n'}^\Gamma(r)$$

The first d near-band-edge states u_n^Γ labeled $n = 1, \ldots, d$ form the set of class-A bands. All remaining states, labeled class-B, are assumed to have only

a small influence on the near band-edge states. Typical number of class-A bands are 1, 4, 6 or 8 [Kan82, Bas88, Chu95, Bah90, MGO94]. The class-B bands are far away from the band-edges E_c and E_v and thus have only a small contribution to a state $u_n(r,k)$ of class-A near zone-center. This gives rise to the representation

$$u_n(r,k) \approx \sum_{n'=1}^{d} c_{n'}(k) u^{\Gamma}_{n'}(r), \quad \text{for } n = 1.\cdots,d, \tag{4}$$

Taking into account remote band effects arising from the influence of the class-B states by means of Löwdins perturbation scheme one arrives at a nonlinear eigenvalue problem for the class-A bands, see [Kan66, Kan82]. A suitable linearization of this problem provides the corresponding Hamiltonian.

In the following we regard eight class-A bands consisting of the lowest conduction band and the three topmost valence bands, all doubly degenerate, see Fig. 3. For materials with diamond or zinc-blende crystallographic structure the space of class-A bands is spanned by $S\uparrow$, $X\uparrow$, $Y\uparrow$, $Z\uparrow$, $S\downarrow$, $X\downarrow$, $Y\downarrow$, $Z\downarrow$, where $\uparrow$ and $\downarrow$ indicate spin up and spin down, respectively. Following the notation of [EW96], the Hamiltonian reads as:

$$H_{8\times 8}(k) = \begin{pmatrix} K(k) + \mathrm{i}\cdot G_z + E & \Gamma \\ \bar{\Gamma} & K(k) - \mathrm{i}\cdot G_z + E \end{pmatrix} \tag{5}$$

where the $k{\cdot}p$ matrix is given by

$$K(k) = \begin{pmatrix} A\cdot k^2 & \mathrm{i}P_0 k_x & \mathrm{i}P_0 k_y & \mathrm{i}P_0 k_z \\ -\mathrm{i}P_0 k_x & (L-M)k_x^2 + Mk^2 & Nk_xk_y & Nk_xk_z \\ -\mathrm{i}P_0 k_y & Nk_xk_y & Lk_y^2 + M(k_x^2+k_z^2) & Nk_yk_z \\ -\mathrm{i}P_0 k_x & Nk_xk_z & Nk_yk_z & Lk_z^2 + M(k_x^2+k_y^2) \end{pmatrix}$$

$$G_z = \frac{\Delta_{so}}{3}\begin{pmatrix} 0&0&0&0 \\ 0&0&-1&0 \\ 0&1&0&0 \\ 0&0&0&0 \end{pmatrix}, \Gamma = \frac{\Delta_{so}}{3}\begin{pmatrix} 0&0&0&0 \\ 0&0&0&1 \\ 0&0&0&-\mathrm{i} \\ 0&-1&\mathrm{i}&0 \end{pmatrix}$$

$$E = \begin{pmatrix} E_g & 0 & 0 & 0 \\ 0 & -\Delta_{so}/3 & 0 & 0 \\ 0 & 0 & -\Delta_{so}/3 & 0 \\ 0 & 0 & 0 & -\Delta_{so}/3 \end{pmatrix}$$

As their influence is usually neglected, the matrix elements describing the influence of bulk inversion asymmetry of potential V_{eff} and the influence of k dependent spin-orbit interaction have been omitted, see [Kan82, Bah90].

The parameters of the Hamiltonian are the (parabolic) conduction band mass m_c, the Luttinger parameters $\gamma_1^L, \gamma_2^L, \gamma_3^L$ describing the the heavy hole masses in different crystallographic directions, the band gap energy E_g, the

spin-orbit split-off energy Δ_{so}, and the momentum matrix element P_0. These parameters define the coefficients of the Hamiltonian by

$$L = -\frac{\hbar^2}{2m_0}(\gamma_1^L + 4\gamma_2^L) + \frac{P_0^2}{E_g}, M = -\frac{\hbar^2}{2m_0}(\gamma_1^L - 2\gamma_2^L), N = -6\frac{\hbar^2}{2m_0}\gamma_3^L + \frac{P_0^2}{E_g} \quad (7)$$

$$A = \frac{\hbar^2}{2m_0}\frac{m_0}{m_c} - P_0^2\frac{E_g + 2/3\Delta_{so}}{E_g(E_g + \Delta_{so})}. \quad (8)$$

P_0 is defined by the Bloch functions S and X

$$P_0 \stackrel{\text{def}}{=} -\mathrm{i}\frac{\hbar}{m_0}\int_{\text{unit cell}} \bar{S}(r)\frac{\hbar}{\mathrm{i}}\frac{\partial}{\partial x}X(r)\,dr, \quad (9)$$

and is a measure for the coupling between the conduction bands and the valence bands. It is also known as the optical matrix element, which plays a role in the calculation of the strength of optical transitions. Usually it is given by an energy parameter

$$E_p = \frac{2m_0}{\hbar^2}P_0^2. \quad (10)$$

It is possible to obtain the parameters E_g,Δ_{so}, m_c, γ_1^L,γ_2^L, γ_3^L and E_p of the Hamiltonian from experimentally determined properties of the bulk material. There exists a compilation [VMRM01] of these band parameters for the 12 major III-V binary semiconductor materials and their ternary and quaternary alloys.

In the literature, also simplified $k{\cdot}p$ Hamiltonians for the valence bands are used. They include the four-band Luttinger-Kohn Hamiltonian for heavy holes and light holes and six-band valence band Hamiltonians [Bas88, Chu95, Car96]. For semiconductors with wurtzite crystallographic structure such as gallium nitride $k{\cdot}p$ Hamiltonians have been established as well [CC96].

2.3 Anomalous band bending

The reciprocal masses A and L on the diagonal of (5) depend on the ratio $\zeta = E_p/E_g$. For $\zeta > \zeta_{crit}$ one of them changes the sign. For large wave vectors k parallel to one of the axis in the k space, these diagonal k^2 terms dominate the behavior of the energy bands. Thus, for $\zeta > \zeta_{crit}$ the energy dispersion becomes anomalous in the sense that e.g. for $A < 0$ the bending of the conduction bands becomes negative, see Fig. 5. It is known, that this behavior of the band structure can lead to the formation of spurious modes, if $k{\cdot}p$ method is applied to heterostructures, see section 3.4 and [For97, Sol03, MGO94].

2.4 Modification of the band structure by mechanical strain

If a semiconductor material is grown on a substrate with a different lattice constant, e.g. indium gallium arsenide on gallium arsenide, we observe mechanical strain induced by the lattice mismatch between the two crystals.

Basically, this mechanical strain leads to a shift of band-edges E_c, E_v resulting in an altered band gap E_g and to a splitting of the heavy hole and light hole bands at the Γ point. Additionally, it has an impact on the anisotropy of the effective mass tensor and the warping of the band structure [CC92].

The influence of strain ε can be included in the $k{\cdot}p$ Hamiltonian by adding the Pikus-Bir deformation interaction matrix $D(\varepsilon)$ defined by deformation potentials [BP74, Bah90, Chu95, EW96].

2.5 Mixed crystal systems

So far, our considerations apply to elementary semiconductors like silicon or binary semiconductors such as gallium arsenide or indium phosphite. Mixed crystal systems are alloys of binary semiconductors. They are of particular interest, because they allow for band gap engineering in the case of ternary compounds like $\mathrm{In}_{1-x}\mathrm{Ga}_x\mathrm{As}$ and additionally for design of the mechanical strain in the case of quaternary materials like $\mathrm{In}_{1-x}\mathrm{Ga}_x\mathrm{As}_y\mathrm{P}_{1-y}$. Though strictly speaking, the basic assumptions of a periodic crystal lattice do not hold for these materials, they can be treated by similar methods assuming the so-called virtual crystal approximation.

Within the kp framework the band structure of mixed crystal systems can be described by the same Hamiltonian used for the elementary and binary semiconductors. Their parameters can be obtained by interpolation of those of the binary constituents. Often linear interpolation according to the mole fraction x yields a sufficient approximation. For some parameters such as the band gap energy E_g this interpolation has to include a bowing parameter. All the related data can be found in [VMRM01].

3 Envelope function approximation for layered semiconductor nanostructures

We have discussed the modeling of the band structure of bulk materials by $k{\cdot}p$ Hamiltonians. Now, this approach is extended to layered semiconductor nanostructures like quantum wells, multiple quantum wells (see Fig. 2) and double barrier structures [Sin93], [Bas88], [Chu95]. For these heterostructures, the translation invariance is broken and the microscopic potential V_{eff} cannot be periodic in all space directions. Nevertheless, the heterostructure is a crystalline solid and the atoms form an approximate Bravis lattice. The microscopic potential now consists of a oscillatory part, which corresponds to the potential of the ionic cores, and a globally slowly varying part, which corresponds to the composition of the heterostructure from different bulk materials, see Fig. 4.

3.1 Envelope function approximation of the wavefunctions

This obvious two-scale nature of the microscopic potential and of the corresponding microscopic wave function encourages to treat this problem as a *multiscale* problem. After first heuristic approaches to this problem, see G. Bastard [Bas88], the first rigourous approach was made by Burt [Bur92, Bur94], who showed, that it is possible to derive a theory for the *slowly-variing* part of the wave functions, the *envelope functions*, in terms of the atomistic scale. This approach leads to a $k{\cdot}p$ Hamiltonian for the envelope functions.

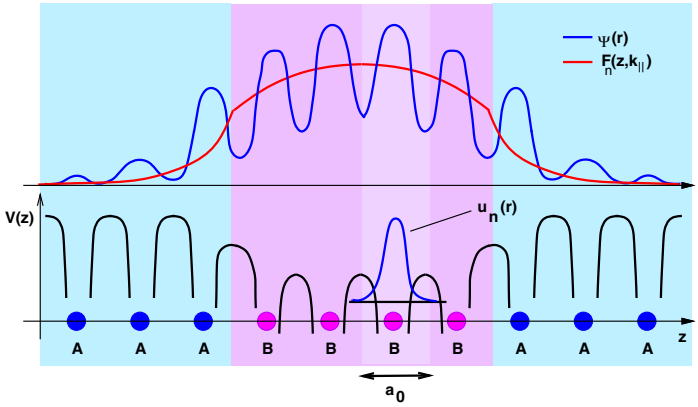

Fig. 4. *Schematic view of the microscopic potential $V(z)$, the atomistic wave function Ψ, the Bloch waves $u_n(r)$ and the envelope function $F(z;k_\parallel)$ in a one-dimensional heterostructure consisting of atoms of type A and B. The lattice constant is a_0 (typically 0.5 nm). $u_n(r)$ is highly oscillatory on the sub-Å-scale.*

For layered nanostructures, the crystal remains periodic in the in-plane directions $r_\parallel = (x, y)$, perpendicular to the growth direction z. This choice of the coordinate system corresponds to epitaxially grown nanostructures on [001] oriented substrates. As in bulk $k{\cdot}p$ theory, we approximate the electronic state in the nanostructure in the subspace spanned by d lattice periodic, zone-center Bloch functions $u_n^\Gamma(r)$, $n = 1, \ldots, d$ of class-A. However, we replace the coefficients c_n in (4) by the envelope functions $F_n(z;k_\parallel)$ depending on the reduced wave vector $k_\parallel = (k_x, k_y)$:

$$\Psi(r;k_\parallel) = \exp(\mathrm{i}k_\parallel \cdot r_\parallel) \sum_{n=1}^{d} F_n(z;k_\parallel) u_n^\Gamma(r).$$

3.2 $k{\cdot}p$-Schrödinger operators for layered nanostructures

According to [Bur92],[Bur94],[Bur99] the vector of the envelope functions $F = (F_1, \cdots, F_d)$ for a given reduced wave vector $k_\parallel$ is the solution of an eigenvalue

problem

$$H\Big(k_\parallel, -\mathrm{i}\frac{\partial}{\partial z}\Big)F(z;k_\parallel) = E(k_\parallel)F(z;k_\parallel). \tag{11}$$

(11) is a family iof spatially one-dimensional eigenvalue problems indexed by $k_\parallel$. It provides a description of the in-plane band structure for layered nanostructures, for examples see section 5.

Far away from the interface between two materials, the Schrödinger operator H is formally identical with the bulk Hamiltonian (replacing $k_z \to -i\partial/\partial z$) shifted by the band-edge E_v [Bur92, Bur94]. Therefore, the band-offset ΔE_v between two materials enters as an additional parameter, available for the many material interfaces [VdW89, Kri91, VMRM01]. Near the interface between two materials, non-local effects are present which lead to a coupling of the states across the interface [Bur92],[Bur94]. The approximation of these non-local interactions by an interface condition for the envelope functions is sufficient for many applications.

However, one has to be aware that the Burt-Foreman approach relies on the assumption that the Bloch functions used in the approximation are the same for all material layers. As a consequence, the momentum matrix element P_0 has the same value in all materials. However, the experimentally measured value of P_0 given by the optical matrix element E_p (10) is varying. Therefore, it is necessary to incorporate this effect in the $k{\cdot}p$ Schrödinger operator by additional interface conditions.

This suggests the following general structure of the Schrödinger operator:

- In each material layer, the Schrödinger operator is derived from a bulk Hamiltonian like (5) resulting in a system of d coupled stationary Schrödinger equations, see (12).
- At the material interfaces the continuity of the envelope functions and of a flux vector (21) is assumed.
- If the optical matrix element P_0 differs only slightly between the materials, one can define an effective value by suitable averaging. Otherwise, by an additional interface condition, one has to define the coupling between the envelope functions related to the Bloch functions S and envelopes related to the Bloch functions X, Y, Z across the interface [Bur99, For97].

The *conventional* $k{\cdot}p$ Schrödinger operators have been derived from the bulk Hamiltonian by replacing $k_z \to -\mathrm{i}\partial/\partial z$, see for instance [Bas88]. This approach also has to be supplemented by coupling conditions at the material interfaces. These interface conditions have been established implicitly using the so-called operator ordering. For the second order terms the BenDaniel-Duke operator ordering $Ak_z^2 \to -\partial/\partial z A(z)\partial/\partial z$ has been used. For the first order terms the heuristic symmetrization rule $Ak_z \to -\frac{\mathrm{i}}{2}[A(z)\partial/\partial z + \partial/\partial z(A(z)\cdot)]$ has been applied [Bas88]. The resulting interface conditions differ from those derived by Burt-Foreman. For a comparison of the different interface conditions see [For93, MGO94].

3.3 Confined states in quantum wells

A quantum well structure consists of a well material layer embedded between two barrier material layers such that band-edge profiles $E_v(z)$ and $E_c(z)$ form a potential well for both holes and electrons, see Fig. 1. This potential well leads to the localization of the carriers in the quantum well region. This effect is known as carrier confinement. Another key feature of quantum wells is the appearance of discrete energy levels due to the size quantization induced by the small width of the quantum well, typically ranging from 2-20 nm. Repeated quantum well structures form multiple quantum wells (MQW), see Fig. 1.

The effect of carrier confinement is utilized in strained multiple-quantum well (SMQW) laser diodes in order to increase the density of states and the material gain in optical active region of the device. The confined carriers in quantum wells are described by the bounded states of the corresponding $k{\cdot}p$ Schrödinger operator (11) which are characterized by the discrete part of the spectrum. The bounded states decay exponentially in the barrier region. Therefore it is possible to use a finite-domain approximation by artificially cutting out a simulation domain Ω and applying homogenous Dirichlet (hard wall) or Neumann (soft wall) boundary conditions.

3.4 Spurious modes

It is known [For97, Sol03] that if the ratio $\zeta = E_p/E_g$, exceeds a critical value ζ_{crit} due to anomalous band bending (see section 2.3) spurious modes occur as eigenfunctions of the $k{\cdot}p$ Schrödinger operator. These spurious modes are concentrated around a large value of k_z, typically outside the first Brillouin zone, and thus spatially oscillatory. The spurious modes lead to a pollution of the spectrum of the operator or even to band gap solutions [For97, Sol03].

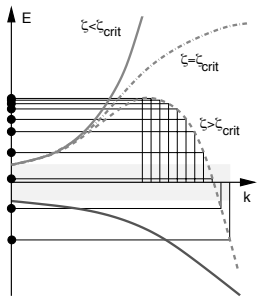

Fig. 5. Schematic view of the dependence of the bending of the energy bands on the ratio $\zeta = E_p/E_g$. In the case $\zeta > \zeta_{crit}$ the bending for large k vectors becomes anomalous. In the case of heterostructures this behavior can lead to pollution of the spectrum by spurious modes or even to band gap solutions, as indicated.

This difficulty can be overcome in several ways:

- Appropriate rescaling of the conduction-valence band coupling to achieve $\zeta < \zeta_{crit}$.
- Fitting of a set of bulk band parameters which ensure $\zeta < \zeta_{crit}$.
- Approximation of the eigenfunctions in a function space which guarantees $k_z < k_{crit}$, k_{crit} is the value for which the bending changes its sign.

[Sti01] achieved a conforming set of band parameters by fitting the Hamiltonian to the real bandstructure in a larger part of the Brilluoin zone (≈20%) and not only at the zone center. These effective parameters meet the conditions given by Property 2 in section 4 which guarantee that there are no spurious modes.

We have obtained a conforming parameter set by rescaling, see section 7.

4 Mathematical analysis of $k{\cdot}p$ Schrödinger operators

We review the spectral properties of Schrödinger type operators occurring in $k{\cdot}p$ theory of layered semiconductor heterostructures. In this section we denote the growth direction of the layers by x and reduced wave vector $k_\parallel$ by $k = (k_1, k_2) \in \mathbb{C}^2$. The formal structure of these operators is – for d bands $\varphi = (\varphi_1, \ldots, \varphi_d)$:

$$\begin{aligned} -\frac{d}{dx}\Big(m_j \frac{\partial}{\partial x}\varphi_j\Big) + \sum_{l=1}^{d}\Big(M_{0\,j\,l}\frac{\partial}{\partial x}\varphi_l - \frac{d}{dx}\Big(\overline{M}_{0\,l\,j}\,\varphi_l\Big)\Big) \\ + \sum_{\alpha=1,2} k_\alpha \sum_{l=1}^{d}\Big(M_{\alpha\,j\,l}\frac{\partial}{\partial x}\varphi_l - \frac{d}{dx}\Big(\overline{M}_{\alpha\,l\,j}\,\varphi_l\Big)\Big) \\ + \sum_{\alpha=1,2} k_\alpha \sum_{l=1}^{d} U_{\alpha\,j\,l}\,\varphi_l + \sum_{\alpha,\beta=1,2} k_\alpha k_\beta \sum_{l=1}^{d} U_{\alpha\,\beta\,j\,l}\,\varphi_l \\ + \sum_{l=1}^{d} v_{j\,l}\,\varphi_l + e_j\varphi_j, \quad j = 1,\ldots d \end{aligned} \tag{12}$$

We assume the following general properties of the coefficients m_j, $M_{0\,j\,l}$, $M_{\alpha\,j\,l}$, $U_{\alpha\,j\,l}$, $U_{\alpha\,\beta\,j\,l}$, $v_{j\,l}$ and e_j on the space intervall $\Omega = (x_0, x_L)$ of the coordinate of quantization:

Property 1. All coefficients are essentially bounded, namely

$$\begin{aligned} m_j &\in L^\infty(\Omega, \mathbb{R}), & j &= 1,\ldots,d, \\ e_j &\in L^\infty(\Omega, \mathbb{R}), & j &= 1,\ldots,d, \\ M_\alpha &\in L^\infty(\Omega; \mathcal{B}(\mathbb{C}^d)), & \alpha &\in \{0,1,2\}, \\ U_\alpha &\in L^\infty(\Omega; \mathcal{B}(\mathbb{C}^d)), & \alpha &\in \{1,2\}, \\ U_{\alpha\,\beta} &\in L^\infty(\Omega; \mathcal{B}(\mathbb{C}^d)), & \alpha,\,\beta &\in \{1,2\}, \\ v &\in L^\infty(\Omega; \mathcal{B}(\mathbb{C}^d)), \end{aligned}$$

where $\mathcal{B}(\mathbb{C}^d)$ is the Banach space of bounded linear operators on $\mathbb{C}^d$.

Property 2. The set of band indices is a disjoint union $\{1,\dots,d\} = D_+ \cup D_-$ of conduction and valence bands that means

$$\min_{j\in D_+} \operatorname*{vraimin}_{x\in\Omega} m_j(x) > 0, \qquad \max_{j\in D_-} \operatorname*{vraimax}_{x\in\Omega} m_j(x) < 0,$$

$$\min_{j\in D_+ l} \operatorname*{vraimin}_{x\in\Omega} e_j(x) > 0, \qquad \max_{j\in D_i} \operatorname*{vraimax}_{x\in\Omega} e_j(x) < 0;$$

D_+ or D_- may be empty. We introduce the conjugation operator Θ on $\mathbb{C}^d$ by

$$\Theta(c_1,\dots,c_d) = (r_1\,c_1,\dots,r_d\,c_d), \quad r_j = \begin{cases} 1 & \text{if } j\in D_+, \\ -1 & \text{if } j\in D_-. \end{cases}$$

Property 3. For almost all $x\in\Omega$ and all $\alpha,\beta\in\{1,2\}$ the operators $U_\alpha(x)$, $U_{\alpha\,\beta}(x)$, and $v(x)$ are selfadjoint over $\mathbb{C}^d$.

Property 4. There is a finite, disjoint partition $x_0 < x_1 < \ldots < x_L$ of the interval $\Omega = (x_0, x_L)$ such that the functions $m_j \in \mathbb{R}$, $j = 1,\dots,d$, and $M_\alpha \in \mathcal{B}(\mathbb{C}^d)$, $\alpha = 0,1,2$, take exactly one value $\widehat{m}_{j,l}$ and $\widehat{M}_{\alpha,l}$, respectively, on each of the intervals $[x_l, x_{l+1})$.

Following [BKKR00] we define parts of the $k{\cdot}p$ Schrödinger operator between $W_0^{1,2} \stackrel{\text{def}}{=} W_0^{1,2}(\Omega;\mathbb{C}^d)$ and its dual space $W^{-1,2}$, the space of anti-linear forms on $W_0^{1,2}$. For $\varphi,\psi\in W_0^{1,2}$ we set

$$\langle H\varphi,\psi\rangle = \sum_{j=1}^{d} \int_\Omega m_j\,\frac{\partial}{\partial x}\varphi_j\,\frac{\partial}{\partial x}\overline{\psi}_j\,dx, \tag{13}$$

$$\langle A_\alpha\varphi,\psi\rangle = \int_\Omega \Big\langle M_\alpha(x)\,\frac{\partial}{\partial x}\varphi(x),\psi(x)\Big\rangle_{\mathbb{C}^d} + \Big\langle M_\alpha^*(x)\,\varphi(x),\frac{\partial}{\partial x}\psi(x)\Big\rangle_{\mathbb{C}^d} dx, \quad \alpha = 0,1,2, \tag{14}$$

$$\langle B_\alpha\,\varphi,\psi\rangle = \int_\Omega \big\langle U_\alpha(x)\,\varphi(x),\psi(x)\big\rangle_{\mathbb{C}^d}\,dx, \qquad \alpha = 1,2, \tag{15}$$

$$\langle B_{\alpha\,\beta}\,\varphi,\psi\rangle = \int_\Omega \big\langle U_{\alpha\beta}(x)\,\varphi(x),\psi(x)\big\rangle_{\mathbb{C}^d}\,dx, \qquad \alpha,\beta = 1,2, \tag{16}$$

$$\langle V\varphi,\psi\rangle = \int_\Omega \big\langle v(x)\,\varphi(x),\psi(x)\big\rangle_{\mathbb{C}^d}\,dx, \tag{17}$$

$$\langle E\varphi,\psi\rangle = \sum_{j=1}^{d} \int_\Omega e_j\,\varphi_j(x)\,\overline{\psi}_j(x)\,dx. \tag{18}$$

Now we define for each reduced wave vector $k = (k_1, k_2) \in \mathbb{C}^2$ the $k{\cdot}p$ Schrödinger operator

$$H_k : W^{-1,2} \to W^{-1,2} \tag{19a}$$

by the sum

$$H_k \;=\; H \,+ A_0 \,+ \sum_{\alpha=1,2} k_\alpha (A_\alpha + B_\alpha) \,+ \sum_{\alpha,\beta=1,2} k_\alpha \, k_\beta \, B_{\alpha\,\beta} \,+\, V \,+\, E. \tag{19b}$$

The terms in (19) relate to (5): E represents the basic energies of the (class A) bands involved; V contains the spin-orbit interaction and the influence of strain; the operators

$$A_0 + \sum_{\alpha=1,2} k_\alpha B_\alpha \qquad \text{and} \qquad H + \sum_{\alpha=1,2} k_\alpha A_\alpha + \sum_{\alpha,\beta=1,2} k_\alpha \, k_\beta \, B_{\alpha\,\beta}$$

describe the first and second order $k{\cdot}p$ interactions, respectively. They represent, e.g. for diamond like crystal structures, interband (interaction within conduction bands and valence bands, respectively) and intraband (interaction between conduction and valence bands) coupling, respectively. Making use of the conjugation operator Θ we can split the Schrödinger operator into intraband and interband coupling terms in the following way:

$$H_{k,intra} = \frac{1}{2}(H_k + \Theta H_k \Theta), \quad H_{k,inter} = \frac{1}{2}(H_k - \Theta H_k \Theta).$$

4.1 Spectral properties

We first state spectral properties of the operator (19) on the space $W^{-1,2}$.

Theorem 5. *See [BKKR00]. We assume Properties 1–4. For any $k \in \mathbb{C}^2$ the operator (19) has the same domain as H, namely $W_0^{1,2}$, and all these operators are closed and have a compact resolvent. For any one dimensional complex analytic submanifold $\mathcal{S}$ of $\mathbb{C}^2$ the operator family $\{H_k\}_{\{k\in\mathcal{S}\}}$ is a holomorphic operator family of type (A), see [Kat84, VII.2]. The spectrum of H_k only consists of at most countably many eigenvalues with finite multiplicity, which do not accumulate at any finite point.*

The restriction of the operator (19) to the space $L^2 \stackrel{\text{def}}{=} L^2(\Omega; \mathbb{C}^d)$ has the following spectral properties.

Theorem 6. *See [BKKR00]. We assume Properties 1–4. The spectra of $H_k|_{L^2}$ and H_k are the same. The resolvent of $H_k|_{L^2}$ is nuclear. For any $k \in \mathbb{C}^2$ the geometric spectral multiplicity is at most d. The domain of $H_k|_{L^2}$ is given by*

$$\mathrm{dom}(H_k|_{L^2}) = W^{1,2} \cap \Big\{ \varphi \;\Big|\; \varphi|_{]x_l,x_{l+1}[} \in W^{2,2}(]x_l, x_{l+1}[),$$
$$\widehat{m}_l \lim_{\substack{x \to x_l \\ x > x_l}} \frac{\partial}{\partial x}\varphi(x) - \widehat{m}_{l-1} \lim_{\substack{x \to x_l \\ x < x_l}} \frac{\partial}{\partial x}\varphi(x) + \big(\widehat{M}^*_{0,l+1} - \widehat{M}^*_{0,l}\big)\varphi(x_l)$$
$$+ \sum_{\alpha=1,2} k_\alpha \big(\widehat{M}^*_{\alpha,l+1} - \widehat{M}^*_{\alpha,l}\big)\varphi(x_l) = 0,\ l = 0, \ldots, L-1 \Big\}. \quad (20)$$

For functions φ from the domain of $H_k|_{L^2}$ the vector

$$m\frac{\partial}{\partial x}\varphi(x) - \big(M^*_0(x) + \sum_{\alpha=1,2} k_\alpha M^*_\alpha(x)\big)\varphi(x) \quad (21)$$

is continuous across the material interfaces.

Theorem 7. *See [BKKR00]. We assume Properties 1–4. If the reduced wave vector $k = (k_1, k_2)$ is from $\mathbb{R}^2$, then the operator $H_k|_{L^2}$ is selfadjoint, has an orthonormal basis of eigenfunctions in L^2, and its geometric and algebraic eigenspaces coincide.*

We now investigate how the spectral properties of the operators $H_k|_{L^2}$ depend on the reduced wave vector k. Unfortunately, the domain of the operators $H_k|_{L^2}$ is not independent of k. Hence, in contrast to Theorem 5, the concept of a holomorphic operator familiy of type (A) does not apply anymore. However we can prove, see [BKKR00], that for any one dimensional complex analytic submanifold $\mathcal{S} \in \mathbb{C}^2$ the family $\{H_k|_{L^2}\}_{k\in\mathcal{S}}$, is an analytic family of operators in the sense of Kato [Kat84, VII.1.2]. This implies that a closed curve, separating two parts of the spectrum of H_k for $k = k_0$, also separates corresponding parts of the spectrum of H_k for k from a suitable neighbourhood of k_0, see [Kat84, Th. VII.1.7].

4.2 Gap estimate

From the point of view of electronic structure calculation it is of interest for which $k \in \mathbb{R}^2$ the spectral gap between the positive and negative parts of the band-edge operator E can be found in the spectrum of H_k, and how one can estimate the size of the gap in terms of k and the data of the problem. This relates also to the problem of spurious modes in bandstructure calculation.

According to Property 2, the lower bound

$$e \stackrel{\mathrm{def}}{=} \min_{j=1,\ldots,d} \operatorname*{vraimin}_{x\in\Omega} |e_j(x)| \quad (22)$$

of the spectral gap in E is positive, and so is the lowest eigenvalue μ of $|H|$. We define the weighted strength of the band couplings by

$$M \stackrel{\mathrm{def}}{=} \frac{\max\limits_{\alpha=1,2} \|M_\alpha\|^2_{L^\infty(\Omega;\mathcal{B}(\mathbb{C}^d))}}{\min\limits_{j=1,\ldots,d} \operatorname*{vraimin}_{x\in\Omega} |m_j(x)|}. \quad (23)$$

Moreover, we assume the following property of the coupling matrix M_0:

Property 8. $M_0(x)$ is skewadjoint and $\Theta M_0(x)$ is selfadjoint for almost all $x \in \Omega$.

Property 8 implies $M_0 + \Theta M_0 \Theta$ that means that the intra-band part of the operator $M_{0,intra}$, see (4), vanishes. This property is satisfied by the usual eight-band Hamiltonian and its heterostructure equivalent, see (5). The skewadjointness of M_0 is a consequence of symmetric operator ordering of the first order terms of conduction-valence band coupling.

Theorem 9. *See [BKKR00]. In addition to Properties 1–4 and Property 8 we assume that for almost all $x \in \Omega$*

$$\Theta U_\alpha(x) \qquad \text{are skewadjoint,} \qquad \alpha \in \{1,2\}, \tag{24}$$

$$\Theta U_{\alpha\,\alpha}(x) \qquad \text{are nonnegative operators,} \qquad \alpha \in \{1,2\}, \tag{25}$$

and

$$\frac{1}{2} \operatorname*{vraimin}_{\eta\in[0,2\pi[,x\in\Omega} \inf \operatorname{spec}\big(\Theta U_\eta(x) + U_\eta(x)\Theta\big) \stackrel{\text{def}}{=} \nu \geq 0, \tag{26}$$

where

$$U_\eta(x) \stackrel{\text{def}}{=} \cos^2\eta U_{11}(x) + \sin^2\eta U_{22}(x) + \sin\eta\cos\eta\big(U_{12}(x) + U_{21}(x)\big).$$

If $|k|$, and λ satisfy the relations

$$0 \;\leq\; \lambda \;\leq\; e - \|v\|_{L^\infty([0,x_L];\mathcal{B}(\mathbb{C}^d))}. \tag{27a}$$

$$|k| \leq \frac{1}{\delta\sqrt{2}} \tag{27b}$$

$$0 < \mu - |k|\sqrt{2}\left(\mu\delta + \frac{M}{\delta}\right) + |k|^2\nu - \|v\|_{L^\infty(\Omega;\mathcal{B}(\mathbb{C}^d))} + e - \lambda, \tag{27c}$$

for some $\delta > 0$, then λ belongs to the resolvent set of H_k.

Thus, we have established a spectral gap $(-\lambda, +\lambda)$ in H_k. In case of $v \equiv 0$ (27c) means that H_k at zone center $k = 0$ has the same spectral gap as the band-edges E. Thus, spurious modes, that means band gap solutions, can be excluded in this case.

By properly choosing δ in (27) one may obtain sharp estimates of the gap, see [BKKR00]. For the optimal choice of $\delta = \delta_{opt}(|k|)$ one obtains the following range of k

$$0 \leq |k|^2 < \frac{e - \|v\|_{L^\infty(\Omega;\mathcal{B}(\mathbb{C}^d))}}{2\,M}. \tag{28}$$

for which a spectral gap in H_k persists.

4.3 Remarks

Apart of $k{\cdot}p$ Schrödinger operators with interband coupling there are also operators with a positive or negative definite main part. In the terms of Property 2 this means that $D_- = \emptyset$ or $D_+ = \emptyset$, respectively. Important examples are the 4-band Luttinger-Kohn-Hamiltonian [Chu95] and 6-band valence band Hamiltonians, see [Car96, CKI94, Chu95, For93, MGO94, Sin93]. If the operator H from (13) is definite, then the operators H_k are semibounded and one obtains more results about the way the eigenvalues and eigenvectors depend on k, see [BKKR00].

The whole theory considerably simplifies, if one relaxes Property 4 such that the coefficient functions M_α, $\alpha = 0, 1, 2$ are continuous. This allows for a regularization of the operators (19). One can prove, see [BKKR00], that the resolvents of a regularizing sequence converge in trace class to the operator (19) with jumping coefficients M_α.

5 Electronic states in strained quantum wells

The band structure in quantum wells is given by the eigenvalue curves $E_i(k_\parallel)$ and the vector of eigenfunctions $F_i(z; k_\parallel) = (F_{i,1}(z; k_\parallel), \ldots, F_{i,d}(z; k_\parallel))$ of the $k{\cdot}p$ Schrödinger operator (11) depending on the reduced wave vector $k_\parallel = (k_x, k_y)$. We regard an eight-band kp Hamiltonian of the type (5) in the formulation given by [EW96]. Thus, the mathematical results of section 4 apply. The numerical calculations have been performed by means of WIAS-QW [BK] using a finite volume method.

In particular, the structure under consideration is a $\mathrm{In}_{1-x}\mathrm{Ga}_x\mathrm{As}_y\mathrm{P}_{1-y}$ based strained MQW structure. The stack consists of six 1% compressively strained 7 nm thick quantum wells ($x = 0.239$, $y = 0.826$), which are separated by 10 nm thick 0.3% tensile strained barriers ($x = 0.291$, $y = 0.539$), see [BHK03]. As confirmed by the calculation of the mini-band formation in the MQW structure [BHK03], the barrier width is such that the lowest states in the wells decouple, that means, they are strongly localized in the individual quantum wells. This allows to restrict ourselves in the following to single quantum well calculations.

5.1 Band structure

Fig. 6 displays the band structure $E_i(k_\parallel)$ for the 7 nm InGaAsP quantum well under consideration. Due to their different effective mass, in quantum wells the confinement energy $E_{conf} = E_{v,qw} - E_i(k_\parallel = 0)$ of the heavy hole states is smaller than for light-hole states ($E_{v,qw}$ is the valence band-edge of the well material). Thus, the degeneracy (at $k = 0$) between light and heavy holes in bulk materials, see Fig. 3, is lifted. The compressive strain increases the splitting between the heavy hole and light hole states while energetically

favoring the heavy holes. Thus, the highest two valence bands correspond to heavy hole states.

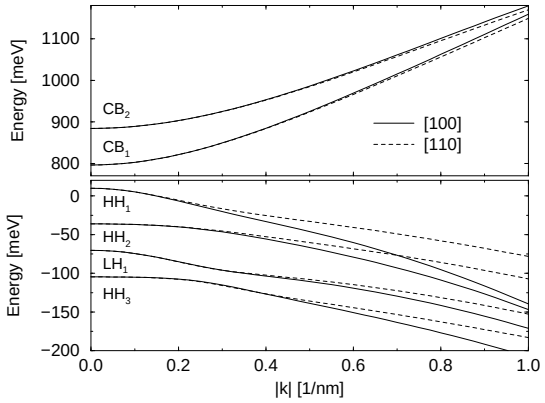

Fig. 6. Band structure and warping in a 7nm InGaAsP compressively strained quantum well, calculated with WIAS-QW. Top: conduction bands, bottom: valence bands. $k_\parallel$ in [100]- (solid) and [110]-direction (dashed). We remark that the bands are twice degenerate due to symmetry. Reprinted with permission from [BHK03]. © 2003, IEEE.

We have investigated two different crystallographic directions to demonstrate the angular dependence of the dispersion (warping effect). We observe weak warping for the conduction band, and strong warping and strong nonparbolicities for the valence bands, see Fig. 6.

5.2 Momentum matrix elements for interband transitions

Important information on the electronic states within the quantum well is encoded in the intersubband momentum matrix elements. For the transition from the conduction band state F_i to the valence band state F_j these are defined, see [EBWS95], by

$$p_{ij} = \frac{m_0}{\hbar} \sum_{\mu,\nu} \int_\Omega \bar{F}_{i,\mu} \Big(\nabla_k H_{\mu\nu}(k_\parallel, k_z) \Big) \Big|_{ik_z = \frac{\partial}{\partial z}} F_{j,\nu} dz. \tag{29}$$

Fig. 7 displays the most prominent interband momentum matrix elements for TE and TM polarization. These momentum matrix elements have a distinctive dispersion and warping. In particular, the dominant transition for TE polarization is between the lowest conduction band CB_1 and the topmost valence band HH_1.

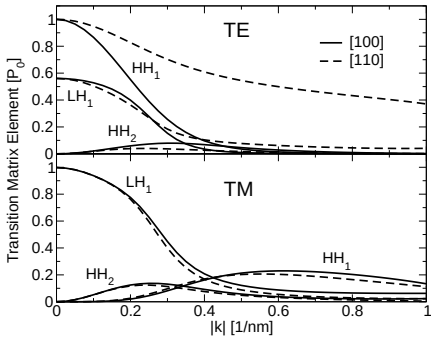

Fig. 7. Momentum matrix element dispersion $|ep_{ij}(k_\parallel)|^2$ (29) for transitions between the lowest conduction band CB_1 shown in Fig. 6 top, and the upper valence bands shown in Fig 6 bottom. Different polarization directions e are shown. Top: TE-polarization ($p||e_x$), bottom: TM-polarization ($p||e_y$). Note the normalization to the same quantity P_0 in both pictures. Reprinted with permission from [BHK03]. © 2003, IEEE.

6 Upscaling to semi-classical state equations

In the simulation of opto-electronic devices such as strained multiple quantum well (SMQW) laser diodes, semi-classical models turned out to be very successful, provided that information about the optical active zone is derived from smaller scale models. This requires suitable *upscaling schemes* for semi-classical constitutive laws.

The simulation of opto-electronic devices requires at least the description of the flow of electrons and holes, the description of the optical field, and the coupling of these models by the radiative recombination of electrons and holes. In the following, we focus on a semi-classical carrier flow model, and on a specific part of radiative recombination; for models of the optical field, see [BGK00, BGH05, BKKR03, BHK03]. In particular, we deal with upscaling schemes for quantities such as the density of states, the optical response, and the optical peak gain, from electronic structure calculations as described in section 5.

6.1 Drift-diffusion equations

The most popular semi-classical models for the carrier flow in a semiconductor device are drift-diffusion models. The basic model of this type is the van Roosbroeck system, see [Gaj93] and the references therein, which describes the flow of electrons and holes in a selfconsistent field due to drift and diffusion. It comprises current–continuity equations for the densities n and p of electrons and holes, respectively, and a Poisson equation for the electrostatic potential φ:

$$q\frac{\partial n}{\partial t} - \nabla \cdot j_n = -qR, \quad q\frac{\partial p}{\partial t} + \nabla \cdot j_p = -qR \tag{30}$$

$$\varepsilon_0 \nabla(\varepsilon_s \nabla\varphi) = -q(C + p - n). \tag{31}$$

ε_0 is the vacuum dielectric constant, ε_s is the static dielectric constant, q is the elementary charge, and C is the net doping. The recombination rate R in (30) involves all non-radiative and radiative recombination processes, and depends at least on n and p. The currents j_n and j_p are driven by the negative gradients of the quasi-Fermi potentials F_n and F_p for electrons and holes, respectively:

$$j_n = -qn\mu_n \nabla F_n, \quad j_p = -qp\mu_p \nabla F_p; \tag{32}$$

μ_n and μ_p are the mobilities of electrons and holes.

The current continuity equations describing the motion of electrons and holes have to be completed by laws for the recombination of electrons and holes, and by Fermi-Dirac distributions for the densities of electrons and holes:

$$n = N_c \mathcal{F}_{1/2}\left(\frac{q\varphi - qF_n - E_c}{k_B T}\right), \quad p = N_v \mathcal{F}_{1/2}\left(\frac{E_v + qF_p - q\varphi}{k_B T}\right). \tag{33}$$

E_c and E_v denote the conduction and valence band edges, respectively. N_c and N_v are the corresponding densities of states (DOS) given by the expressions

$$N_c = 2\left(\frac{m_c k_B T}{2\pi\hbar^2}\right)^{3/2}, \quad N_v = 2\left(\frac{m_v k_B T}{2\pi\hbar^2}\right)^{3/2}. \tag{34}$$

m_c and m_v are the density of state masses, T is the temperature, k_B is Boltzmann's constant, and $\mathcal{F}_{1/2}$ Fermi's integral of the order 1/2:

$$\mathcal{F}_{1/2}(x) = \frac{2}{\sqrt{\pi}} \int_0^\infty \frac{\sqrt{y}}{1 + \exp(y - x)} dy. \tag{35}$$

The constitutive equations link the classical drift-diffusion equations to the quantum mechanical model for the electronic structure. Typically one derives parameters in a constitutive law by upscaling of electronic structure information. Examples are the band-edges E_c, E_v and the density of states N_c, N_v.

6.2 Effective band-edges and densities of states

In the flat-band case, $q\varphi - qF_n$ and $q\varphi - qF_p$ are approximately constant across the nanostructure. Therefore, we can define the quasi Fermi levels of the quantum confined electrons and holes by $E_{Fn} = q\varphi - qF_n$ and $E_{Fp} = q\varphi - qF_p$, respectively. SMQW lasers are usually designed such that they operate in this

flat-band mode. Assuming thermodynamic equilibrium of confined electrons and holes, respectively, their local density distributions for given quasi Fermi levels E_{Fn} and E_{Fp} are calculated by

$$n_{qw}(z) = \sum_{i\in c} \frac{1}{2\pi^2} \int f\Big(E_i(k_\parallel) - E_{Fn}\Big) \|F_i(z;k_\parallel)\|^2_{\mathbb{C}^d}\, dk_\parallel, \tag{36}$$

$$p_{qw}(z) = \sum_{j\in v} \frac{1}{2\pi^2} \int f\Big(E_{Fp} - E_j(k_\parallel)\Big) \|F_j(z;k_\parallel)\|^2_{\mathbb{C}^d}\, dk_\parallel, \tag{37}$$

with Fermi's function

$$f(E) = \left(1 + \exp\left(\frac{E}{k_B T}\right)\right)^{-1}. \tag{38}$$

We introduce the *average* carrier densities per quantum well by $\bar{n} = \int_\Omega n_{qw}(z)dz/d_{qw}$ and $\bar{p} = \int_\Omega p_{qw}(z)dz/d_{qw}$, where d_{qw} is the thickness of the well. For our example quantum well structure from section 5 the local carrier distributions are plotted in Fig. 8 for different values of the sheet concentrations $N = \bar{n}\, d_{qw}$ and $P = \bar{p}\, d_{qw}$.

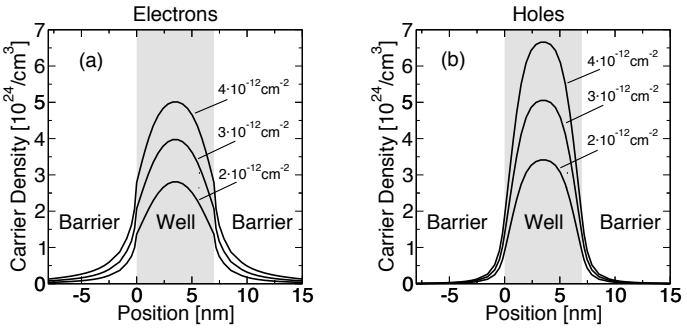

Fig. 8. Local carrier density distributions (36) and (37) for different values of the sheet concentrations $N = P = 2{\cdot}10^{-12}cm^{-2}, 3{\cdot}10^{-12}cm^{-2}, 4{\cdot}10^{-12}cm^{-2}$ for ambient temperature. One observes a stronger confinement of the holes in comparison to the electrons.

For a calculated band structure we regard the averaged carrier densities in their dependence on E_{Fn}, E_{Fp} and k_BT:

$$\bar{n} = \bar{n}\,(E_{Fn}, k_B T)\,, \quad \bar{p} = \bar{p}\,(E_{Fp}, k_B T)\,, \tag{39}$$

see Fig. 9 and Fig. 10 for our example. These relations are fitted to the Fermi-Dirac distributions

$$\bar{n} = N_c \mathcal{F}_{1/2}\left(\frac{E_{Fn} - E_c}{k_B T}\right), \tag{40}$$

$$\bar{p} = N_v \mathcal{F}_{1/2}\left(\frac{E_v - E_{Fp}}{k_B T}\right) \tag{41}$$

by adjusting the parameters N_c,E_c and N_v, E_v for a specified reference temperature T_0. By (34) we obtain the density of state masses m_c and m_v. This procedure provides quantum corrected band-edges E_c, E_v and density of state masses m_c and m_v. Thus, one can treat individual quantum wells as an artificial classical material, whose parameters significantly differ from bulk values of the quantum well materials. This approach has been applied to the the

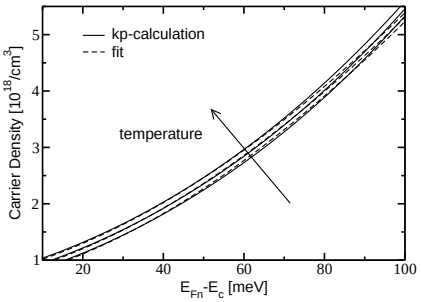

Fig. 9. Relation (39) (kp-calculation) between electron density n and Fermi level E_{Fn} relative to the net band edge E_c for temperatures T=290K, 315K, 340K. The dashed lines indicate the fit to the macroscopic state-equation (40). Reprinted with permission from [BHK03]. © 2003, IEEE.

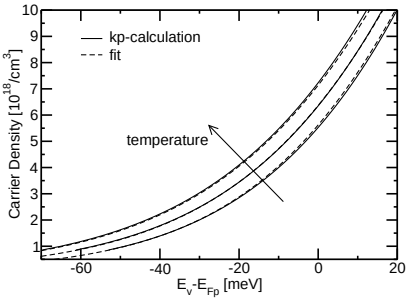

Fig. 10. Relation (39) (kp-calculation) between hole density p and Fermi level E_{Fp} relative to the net band edge E_v for temperatures T=290K, 315K, 340K. The dashed lines indicate the fit to the macroscopic state-equation (41). Reprinted with permission from [BHK03]. © 2003, IEEE.

MQW structure discussed in section 5. Fig. 10 and Fig. 9 demonstrate the high quality of the fit for this particular structure [BHK03].

6.3 Material gain

Still assuming the flat-band conditions, the band structure and the momentum matrix elements (29) enter the expression for the material gain

$$g(\omega) = \frac{\pi\hbar q^2}{\varepsilon_0 m_0^2 n_r c}\frac{1}{d_{qw}}\frac{1}{4\pi^2}\sum_{\substack{i\in c\\ j\in v}}\int \frac{|p_{ij}e|^2}{E_i - E_j} f(E_i - E_{Fn})\,(1 - f(E_j - E_{Fp}))\times \left[1 - \exp\left(\frac{\hbar\omega - (E_{Fn} - E_{Fp})}{k_B T}\right)\right]\frac{1}{\pi}\frac{\Gamma}{\left[(E_i - E_j) - \hbar\omega\right]^2 + \Gamma^2}\,dk_{\|}, \tag{42}$$

where the last factor includes broadening due to collision processes [End97]. The latter have been parametrized by a characteristic intra-band relaxation time τ of 60 fs ($\Gamma = \hbar/\tau$). c is the speed of light and n_r the refractive index.

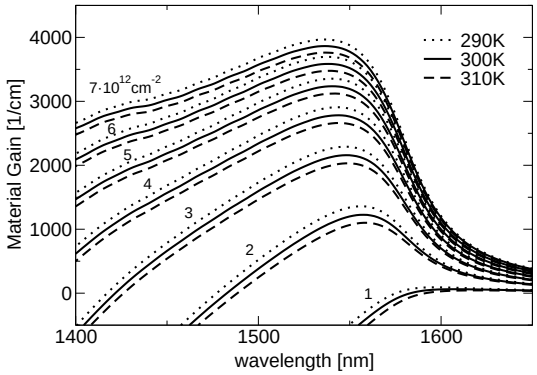

Fig. 11. Material gain spectra (TE-polarization) according to (42) for different sheet concentrations and temperatures. Reprinted with permission from [BHK03]. © 2003, IEEE.

For the case of an undoped active region and local charge neutrality the calculated gain spectra are drawn in Fig. 11 for different excitations and temperatures. The evolution of the corresponding maximum material gain with the carrier density shown in Fig. 12 for different temperatures. In [BHK03] it is discussed how to fit the calculated peak gain characteristics to a logarithmic model $g(n) = g_0 \log(n/n_t)$, which is used as a state equation in semi-classical equations.

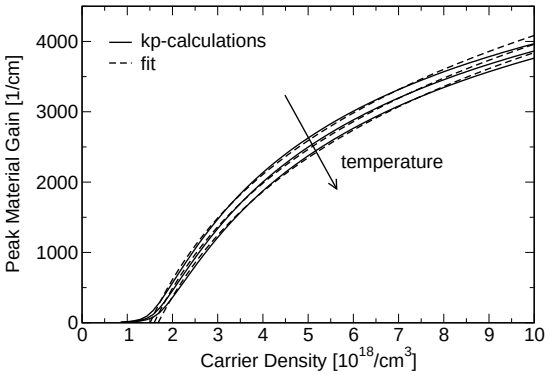

Fig. 12. Maximum material gain for different carrier densities and temperatures T=290K, 300K, 310K. Dashed lines indicate the fit to the logarithmic gain model $g(n) = g_0 \log(n/n_t)$. Whereas $g_0 = 2155\text{cm}^{-1}$ is not very sensitive to the temperature and has been kept constant here, the transparency density $n_t = n_t(T)$ roughly linearly increases with the temperature. Reprinted with permission from [BHK03]. © 2003, IEEE.

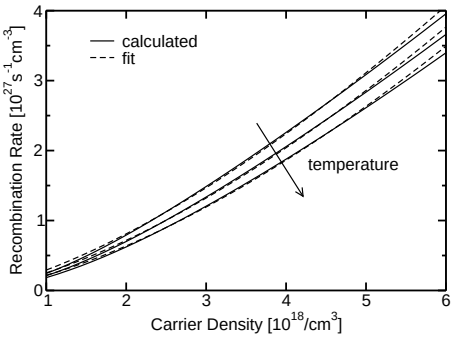

Fig. 13. Spontaneous radiative recombination rate (43) for different temperatures T=290K, 315K, 340K. Dashed: fit to $R_{rad} = Bn^{\alpha}$, with $\alpha = 1.47\ (290K), 1.51\ (315K), 1.55\ (340K)$. Reprinted with permission from [BHK03]. © 2003, IEEE.

6.4 Spontaneous radiative recombination rate

The spontaneous radiative recombination rate R_{rad} is calculated according to [Wen] by

$$R_{rad} = \frac{n_r q^2}{\pi\hbar^2 c^3 \varepsilon_0 m_0^2} \frac{1}{d_{qw}} \frac{1}{4\pi^2} \sum_{\substack{i\in c \\ j\in v}} \int (E_i - E_j) \left|p_{ij}\right|^2 \times f(E_i - E_{Fn}) f(E_{Fp} - E_j)\, dk_{\|}. \tag{43}$$

It is shown in Fig. 13 together with the fit to $R_{rad} = Bn^{\alpha}$. The exponent was approximately $\alpha = 1.5$ which differs from the commonly used models corresponding to $\alpha = 2$.

7 Avoiding spurious modes by adjusting E_p

For low band gap semiconductors, the parameters of the eight-band Hamiltonian often cause anomalous band bending, see section 2.3. This may lead to spurious modes of the $k{\cdot}p$ Schrödinger operator for heterostructures, see section 3.4. However, it is possible to fullfil the condition $\zeta < \zeta_{crit}$ by lowering the value of E_p (10):

$$E_p \to E_p' = \alpha E_p, \quad \alpha < 1 \tag{44}$$

This adjustment has only a small influence on the band structure for low values of k and therefore leaves the confined states nearly untouched.

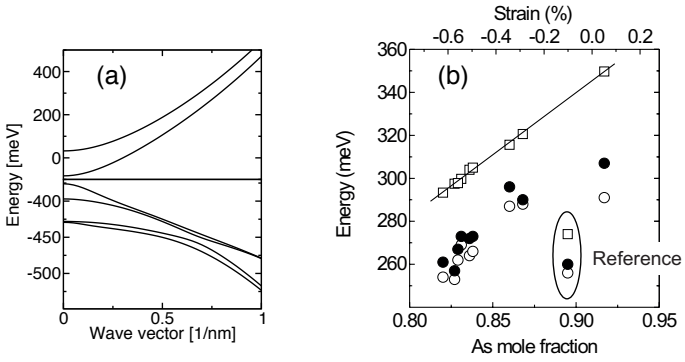

Fig. 14. (a) Calculated conduction and valence band structures for a $InAs_xSb_{1-x}/GaSb$ quantum well with the As mole fraction of $x = 0.82$ at ambient temperature, see [KBB+05]. (b) Comparison between eight-band $k{\cdot}p$–band structure calculations and experiments for a set of InAsSb/GaSb multiple quantum well samples with different As mole fractions. Full circles indicate the MQW–edge as determined from transmittance, whereas open circles point to the edge as deduced from PL. Squares mark the edge as obtained from the energy difference of the lowest conduction band (at $k = 0$) and the highest valence band (at $k = 0$) according to 8–band $k{\cdot}p$–calculations. One observes a systematic IR-shift of the QW–edge data experimentally determined compared to the $k{\cdot}p$ calculation. This tendency is also present in the $InAs_{0.895}Sb_{0.105}$ bulk–like sample, indicated as 'Reference'. Thus it is not likely to be a residual effect of the $k{\cdot}p$ calculation. (b) reprinted with permission from [KBB+05]. © 2005 American Institute of Physics.

In the limit case $E_p \to 0$ the conduction bands and the valence bands decouple, and one arrives at the usual six-band Hamiltonian for valence band

states. This Hamiltonian still provides a reasonable approximation of the valence band structure [CC92, For93, MGO94, CC96].

The $InAs_xSb_{1-x}$ system is the alloy with the lowest direct band–gap value of all III–V–semiconductor materials. This mixed crystal system is of utmost interest for infrared (IR) optoelectronic applications such as heterostructure–based lasers and detectors [WGS+00, GKS00]. In [KBB+05] the rescaling approach is applied to the calculation of the electronic states in a set of samples with different mole fractions x. For a comparison of eight-band $k{\cdot}p$ calculation with the experimentally measured properties of the samples, see Fig. 14.

8 Biased quantum wells

Typical applications of biased quantum well structures are photonic integrated chips consisting of integrated semiconductor laser/electro-absorption modulator [Bas95, Ch. 6], [Chu95, Ch. 13]. In such devices, the external electric field allows to modulate the absorption or the reflectivity for specific spectral regions.

The applied voltage leads to tilted band edges in the quantum well region, hence, to meta-stable states. If the applied bias is small with respect to the band-edge offsets ΔE_v and ΔE_c of the quantum well to the barrier, then hard wall or soft wall boundary conditions can still be applied for the calculation of the electronic states [SB87, DF93, ASV98]. The calculated eigenvalues $E_i(k_\parallel)$ yield an reasonable approximation of the real parts of the complex eigenvalues corresponding to the meta-stable states of the biased structure.

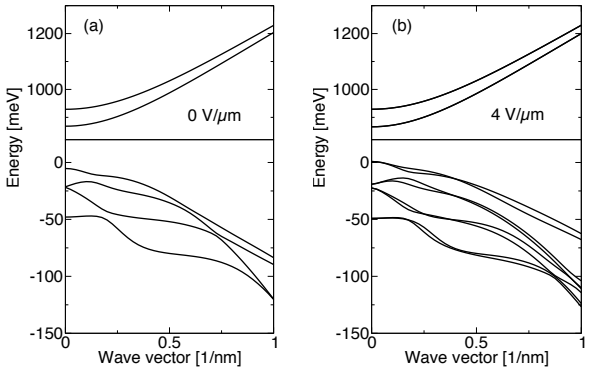

Fig. 15. Band structure ([100] direction) in a 13 nm InGaAsP quantum well lattice-matched to InP barriers for two different external electric fields. (a) F=0 V/μm, and (b) F=4 V/μm. At F=0 V/μm, the valence bands are double degenerate. At F=4 V/μm, they split due to the applied external electric field (Rashba effect).

As an example we discuss the application of this approach to the calculation of the band structure and the local carrier density distributions for a 13 nm thick InGaAsP quantum well, lattice-matched to InP barriers. In Figs. 15 and 16 we present the results of eight-band $k{\cdot}p$ calculations for various values of the electrical field. Due to the Kramers degeneracy the heavy and light hole bands are double degenerate for an unbiased quantum well, see Fig. 15a. This spin degeneracy is lifted if an electric field is applied to the quantum well, see Fig. 15b. The spin splitting of the valence bands induced by the external electric field is known as the Rashba effect.

Fig. 16 shows titled band edge profiles and carrier density distributions for different applied biases. For the electric field strength $F = 6$ V/μm one observes the onset of accumulation of the hole density in the barrier region, marking the limit of the approach based on the use of hard wall boundary conditions.

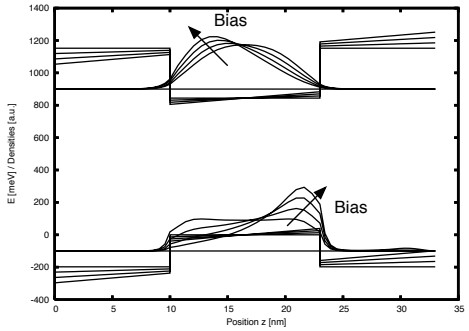

Fig. 16. Tilted band edge profiles $E_c(z)$ and $E_v(z)$ and local density distributions for electrons and holes in a 13 nm InGaAsP quantum well lattice-matched to InP barriers for different external electric fields. F=0 V/μm, 2 V/μm, 4 V/μm, 6 V/μm.

References

[ASV98] A. Ahland, D. Schulz, and E. Voges. Efficient modeling of the optical properties of MQW modulators on InGaAsP with absorption edge merging. *IEEE Journal of Quantum Electronics*, 34, 1597–1603, 1998.

[Bah90] T. B. Bahder. Eight-band $k \cdot p$ model of strained zinc-blende crystals. *Physical Review B*, 41(17), 11992–12001, 1990.

[Bas88] G. Bastard. *Wave Mechanics applied to Semiconductor Heterostructures*. Halsted Press, 1988.

[Bas95] M. Bass, editor. *Handbook of optics. 2. Devices, measurement, and properties*. McGraw-Hill, New York, 1995.

[BGH05] U. Bandelow, H. Gajewski, and R. Hünlich. Fabry–Perot Lasers: Thermodynamics-Based Modeling. In J. Piprek, editor, *Optoelectronic Devices*. Springer, 2005.

[BGK00] U. Bandelow, H. Gajewski, and H.-C. Kaiser. Modeling combined effects of carrier injection, photon dynamics and heating in Strained Multi-Quantum Well Lasers. In M. O. Rolf H. Binder, Peter Blood, editor, *Physics and Simulation of Optoelectronic Devices VIII*, volume 3944 of *Proceedings of SPIE*, pages 301–310, August 2000.

[BHK03] U. Bandelow, R. Hünlich, and T. Koprucki. Simulation of Static and Dynamic Properties of Edge-Emitting Multiple-Quantum-Well Lasers. *IEEE Journal of Selected Topics in Quantum Electronics*, 9, 798–806, 2003.

[BK] U. Bandelow and T. Koprucki. WIAS-QW. Online: http://www.wias-berlin.de/software/qw.

[BKKR00] U. Bandelow, H.-C. Kaiser, T. Koprucki, and J. Rehberg. Spectral properties of $k \cdot p$ Schrödinger operators in one space dimension. *Numerical Functional Analysis and Optimization*, 21, 379–409, 2000.

[BKKR03] U. Bandelow, H.-C. Kaiser, T. Koprucki, and J. Rehberg. Modeling and simulation of strained quantum wells in semiconductor lasers. In W. Jäger and H.-J. Krebs, editors, *Mathematics - Key Technology for the Future. Joint Projects Between Universities and Industry*, pages 377–390. Springer Verlag, Berlin Heidelberg, 2003.

[Blo32] F. Bloch. Über die Quantenmechanik der Electronen in Kristallgittern. *Z. Physik*, 52, 555–600, 1932.

[BP74] G. L. Bir and G. E. Pikus. *Symmetry and Strain-Induced Effects in Semiconductors*. John Wiley & Sons, New York, 1974. Übersetzung aus dem Russischen von P. Shelnitz.

[Bur92] M. G. Burt. The justification for applying the effective-mass approximation to microstructures. *J. Physics. Condens. Matter*, 4, 6651–6690, 1992.

[Bur94] M. G. Burt. Direct derivation of effective-mass equations for microstructures with atomically abrupt boundaries. *Physical Review B*, 50(11), 7518–7525, 1994.

[Bur99] M. G. Burt. Fundementals of envelope function theory for electronic states and photonic modes in nanostructures. *J. Physics. Condens. Matter*, 11, R53–R83, 1999.

[Car96] M. Cardona. *Fundamentals of Semiconductors*. Springer, Berlin, 1996.

[CB66] M. L. Cohen and T. K. Bergstresser. Band Structures and Pseudopotential Form Factors for Fourteen Semiconductors of the Diamond and Zinc-blende Structures. *Phys. Rev.*, 141, 789–796, 1966.

[CC76] J. R. Chelikowsky and M. L. Cohen. Nonlocal pseudopotential calculations for the electronic structure of eleven diamond and zinc-blende semiconductors. *Phys. Rev. B*, 14, 556–582, 1976.

[CC92] C. Y.-P. Chao and S. L. Chuang. Spin-orbit-coupling effects on the valence-band structure of strained semiconductor quantum wells. *Physical Review B*, 46(7), 4110–4122, 1992.

[CC96] S. L. Chuang and C. S. Chang. k·p method for strained wurtzite semiconductors. *Phys. Rev. B*, 54, 2491–2504, 1996.

[Chu95] S. L. Chuang. *Physics of optoelectronic Devices*. Wiley & Sons, New York, 1995.

[CKI94] W. W. Chow, S. W. Koch, and M. S. III. *Semiconductor–Laser Physics*. Springer–Verlag, Berlin, 1994.

[DF93] P. Debernardi and P. Fasano. Quantum confined Stark effect in semiconductor quantum wells including valence band mixing and Coulomb effects. *IEEE Journal of Quantum Electronics*, 29, 2741–2755, 1993.

[EBWS95] P. Enders, A. Bärwolff, M. Woerner, and D. Suisky. $k \cdot p$ theory of energy bands, wave functions and optical selection rules in strained tetrahedral semiconductors. *Physical Review B*, 51(23), 16695–16704, 1995.

[End97] P. Enders. Enhancement and spectral shift of optical gain in semiconductors from non–markovian intraband relaxation. *IEEE Journal of Quantum Electronics*, 33(4), 580–588, 1997.

[EW96] P. Enders and M. Woerner. Exact 4×4 block diagonalization of the eight-band $k \cdot p$ Hamiltonian matrix for tetrahedral semiconductors and its application to strained quantum wells. *Semicond. Sci. Technol.*, 11, 983–988, 1996.

[For93] B. A. Foreman. Effective-mass Hamiltonian and boundary conditions for the valence bands of semiconductor microstructures. *Physical Review B*, 48(7), 4964–4967, 1993.

[For97] B. A. Foreman. Elimination of spurious solutions from eight-band $k \cdot p$ theory. *Physical Review B*, 56(20), R12748–R12751, 1997.

[Gaj93] H. Gajewski. Analysis und Numerik von Ladungstransport in Halbleitern (Analysis and numerics of carrier transport in semiconductors). *Mitt. Ges. Angew. Math. Mech.*, 16(1), 35–57, 1993.

[GKS00] H. H. Gao, A. Krier, and V. V. Sherstnev. *Appl. Phys. Lett.*, 77, 872, 2000.

[Kan66] E. O. Kane. The $k \cdot p$ Method. In R. K. Willardson and A. C. Beer, editors, *Semiconductors and Semimetals*, volume 1, chapter 3, pages 75–100. Academic Press, New York and London, 1966.

[Kan82] E. O. Kane. Energy Band Theory. In W. Paul, editor, *Handbook on Semiconductors*, volume 1, chapter 4a, pages 193–217. North-Holland, Amsterdam, New York, Oxford, 1982.

[Kat84] T. Kato. *Pertubation theory for linear operators*, volume 132 of *Grundlehren der mathematischen Wissenschaften*. Springer Verlag, Berlin, 1984.

[KBB+05] T. Koprucki, M. Baro, U. Bandelow, T. Tien, F. Weik, J. Tomm, M. Grau, and M.-C. Amann. Electronic structure and optoelectronic properties of strained InAsSb/GaSb multiple quantum wells. *Appl. Phys. Lett.*, 87, 81911/1–181911/3, 2005.

[Kri91] M. P. C. M. Krijn. Heterojunction band offsets and effective masses in III-V quarternary alloys. *Semicond. Sci. Technol.*, 6, 27–31, 1991.

[MGO94] A. T. Meney, B. Gonul, and E. P. O'Reilly. Evaluation of various approximations used in the envelope-function method. *Physical Review B*, 50(15), 10893–10904, 1994.

[SB87] G. D. Sanders and K. K. Bajaj. Electronic properties and optical-absorption spectra of GaAs-$Al_xGa_{1-x}As$ quantum wells in externally appield electric fields. *Phys. Rev. B*, 35, 2308–2320, 1987.

[Sin93] J. Singh. *Physics of semiconductors and their heterostructures*. McGraw–Hill, New York, 1993.

[Sol03] X. C. Soler. *Theoretical Methods for Spintronics in Semiconductors with Applications*. PhD thesis, California Institute of Technology, Pasadena, California, USA, 2003.

[Sti01] O. Stier. *Electronic and Optical Properties of Quantum Dots and Wires*. Dissertation TU Berlin, Germany. Wissenschaft & Technik Verlag, Berlin, 2001.

[VdW89] C. G. Van de Walle. Band lineups and deformation potentials in the model-solid theory. *Phys. Rev. B*, 39, 1871–1883, 1989.

[VMRM01] I. Vurgaftman, J. R. Meyer, and L. R. Ram-Mohan. Band parameters for III-V compound semiconductors and their alloys. *J. Appl. Phys.*, 89, 5815–5875, 2001.

[Wen] H. Wenzel. How to use the kp8 programs. Online: http://www.fbh-berlin.de/people/wenzel/kp8.html.

[WGS+00] A. Wilk, M. E. Gazouli, M. E. Skouri, P. Cristol, P. Grech, A. N. Baranov, and A. Joullie. *Appl. Phys. Lett.*, 77, 2298, 2000.